J|A|C|S
ARTICLES
Published on Web 04/27/2004

Permanent Microporosity and Enantioselective Sorption in a Chiral Open Framework

Darren Bradshaw, Timothy J. Prior, Edmund J. Cussen, John B. Claridge, and Matthew J. Rosseinsky*

Contribution from the Department of Chemistry, University of Liverpool, Liverpool L69 7ZD, United Kingdom

Received December 11, 2003; E-mail: m.j.rosseinsky@liv.ac.uk

Abstract: A homochiral microporous material is presented. The phase has 47% permanently porous void volume and is shown to have >1 nm diameter pores with three-dimensional channels using probe molecule sorption. Enantioselective guest sorption is strongly dependent on guest size. The homochiral microporous phase was identified by reactive selection from a first-generation chiral but nonporous framework. Chiral permanent porosity is established by directional noncovalent interactions between framework-forming and nonframework forming components of the stable second-generation material, which become stronger upon loss of the guests from the pore system.

Introduction

Chirality and porosity play important roles in chemistry and biology. It is challenging to design a crystalline material combining both properties.[1] Microporous materials have pores of up to 2 nm in dimension and display permanent porosity due to the retention of their structural integrity in the absence of a guest.[2] The classical examples of these materials are the aluminosilicate zeolites, which have widespread industrial applications due to the stability conferred by the strength of the Si−O bond and the excellent size selectivity offered by the narrow pore size distribution in the crystalline material, but thus far, no homochiral microporous systems have been reported. Although considerable progress has been made in guest-exchange and catalysis with crystalline metal-organic open-framework chiral materials that collapse or change structure on guest-removal,[3−5] these systems are not microporous as the extensive channels in the structures close when the guests occupying them are removed. Mesoporous amorphous inorganic−organic hybrids can display enantioselective catalytic hydrogenation activity.[6,7] The development of strategies to confer permanent porosity on homochiral crystalline solids with nanometer-sized channels is important for the discovery of new generations of chiral catalysts and sorbents.

Here, we report the identification and bulk synthesis of a homochiral permanently microporous material with a three-dimensional channel system that retains crystallinity upon guest loss and displays enantioselective sorption of guests with dimensions that approach the pore size. Refinement of the guest-free structure allows identification of the chemical interactions conferring stability on the open framework. Direct pore size determination by sorption of a range of probe molecules reveals that the pores are larger than 10.5 Å. The retention of porosity on guest loss results from the presence of a subtle interaction, identified by reactive selection, stabilizing the framework over apparently similar systems that collapse and do not retain porosity upon guest removal.

Metal-organic open frameworks, constructed by the coordination of a multidentate ligand molecule to a metal center, have undergone explosive development recently,[8−10] driven by the precise control the structure and chemistry[11] of the molecular precursors offer in the design of the resulting open framework materials.[12] Chirality can be imparted on such structures using chiral molecular building blocks as the nodes of the networks.[13−15] Three-connected three-dimensional nets offer an alternative mechanism for imposing chirality as the topology of such frameworks is often chiral due to the presence of helices[16] in the extended structures.[17] An example of this is the (10,3)-a network which contains both 3-fold and 4-fold helices. The

(1) Davis, M. E. *Nature* **2002**, *417*, 813−821.
(2) Rouquerol, J.; Avnir, D.; Fairbridge, C. W.; Everett, D. H.; Haynes, J. H.; Pericone, N.; Ramsay, J. D. F.; Sing, K. S. W.; Unger, K. K. *Pure Appl. Chem.* **1994**, *66*, 1739−1758.
(3) Seo, J. S.; Whang, D.; Lee, H.; Jun, S. I.; Oh, J.; Jeon, Y. J.; Kim, K., *Nature* **2000**, *404*(6781), 982−986.
(4) Cui, Y.; Evans, O.; Ngo, N.; White, P.; Lin, W. *Angew. Chem., Int. Ed.* **2002**, *41*(7), 1159.
(5) Xiong, R.-G.; You, X.-Z.; Abrahams, B. F.; Xue, Z.; Che, C.-M., *Angew. Chem., Int. Ed.* **2001**, *40*, 4422−4423.
(6) Hu, A.; Ngo, H. L.; Lin, W. *J. Am. Chem. Soc.* **2003**, *125*, 11490−11491.
(7) Saiki, T.; Dewa, T.; Aoyama, Y. *Mol. Cryst. Liquid Cryst.* **2000**, *342*, 241−248.
(8) Yaghi, O.; O'Keeffe, M.; Ockwig, N.; Chae, H.; Eddaoudi, M.; Kim, J. *Nature* **2003**, *423*(6941), 705−714.
(9) Robson, R. *J. Chem. Soc., Dalton Trans.* **2000**, 3735−3744.
(10) Moulton, B.; Zaworotko, M. J. *Curr. Opin. Solid State Mater. Sci.* **2002**, *6*, 117−123.
(11) Kitaura, R.; Kitagawa, S.; Kubota, Y.; Kobayashi, T. C.; Kindo, K.; Mita, Y.; Matsuo, A.; Kobayashi, M.; Chang, H. C.; Ozawa, T. C.; Suzuki, M.; Sakata, M.; Takata, M. *Science* **2002**, *298*(5602), 2358−2361.
(12) Pan, L.; Ching, N.; Huang, X.; Li, J. *Inorg. Chem.* **2000**, *39*, 5333−5340.
(13) Cui, Y.; Lee, S. J.; Lin, W. *J. Am. Chem. Soc.* **2003**, *125*, 6014−6015.
(14) Robson, R.; Abrahams, B. F.; Moylan, M.; Orchard, S. D. *Angew. Chem., Int. Ed.* **2003**, *42*, 1848−1851.
(15) Pschirer, N. G.; Ciurtin, D. M.; Smith, M. D.; Bunz, U. H. F.;zur Loye, H. C. *Angew. Chem., Int. Ed.* **2002**, *41*, 583−585.
(16) Gier, T. E.; Bu, X.; Feng, P.; Stucky, G. D. *Nature* **1998**, *395*, 154−156.
(17) Batten, S. R.; Robson, R. *Angew. Chem., Int. Ed.* **1998**, *110*, 1558−1595.

10.1021/ja0316420 CCC: $27.50

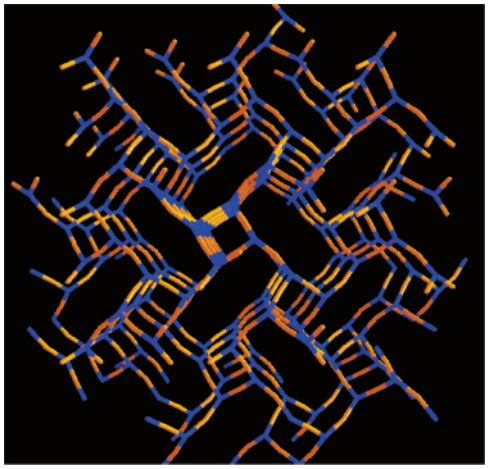

Figure 1. The chiral (10,3)-a M_3btc_2 network which is the basic structural unit of **I** and **II**, showing the helical motifs along the cube edge direction. The gold, M centers are linear connectors and the blue btc centers produce the three connectivity. Figure S1 shows the network viewed along ⟨111⟩. Two of these nets interpenetrate in 2×(10,3)-a phases **I** and **II** (Figure 3) and the arrangement of the auxiliary ligands completing the octahedral coordination at M in Figure 4.

network is so-called because the smallest closed loop m described by the n-connected nodes of the (m,n) network is a decagon. The network can be generated by binding the tridentate 1,3,5-benzenetricarboxylate (btc) ligand to transition metal cations. The handedness (sense of rotation) of these intrinsically chiral M_3btc_2 ($M = Ni^{2+}$, Co^{2+}) networks (Figure 1) can be controlled by the chirality of a small templating bidentate alcohol molecule (such as propan-1,2-diol, 1,2-pd) bound to the metal center M.[18] As M is octahedrally coordinated and acts as a linear connector between two trans btc ligands, there are four sites available to nonframework-forming auxiliary ligands. This gives an overall composition $M_3btc_2X_6Y_3$·[guests], where auxiliary ligand X is a nitrogen heterocycle (pyridine, py, in the first generation of chiral open frameworks referred to as **I** here), auxiliary ligand Y the bidentate diol template and [guests] refer to those species residing in the channels of the structure. This affords solids containing helices with only one single hand and thus of unique chirality, controlled by the hand of the diol. The structures contain two interpenetrating (10,3)-a networks with the same chirality, referred to as 2 × (10,3)-a phases. It is particularly challenging to render networks with chiral topologies robust to guest loss and this paper focuses on the identification of mechanisms to render this class of materials microporous.

Experimental Section

Synthesis. The preparation of the non−porous first generation frameworks **I** $Ni_3btc_2(py)_6(1,2\text{-pd})_3$·$[(1,2\text{-pd})_{11}(H_2O)_8]$ is described in ref 18. All chemicals used in the synthesis of the second generation porous frameworks **II** were as purchased from the Aldrich Chemical Co. unless stated in parentheses within the text. Nickel (II) nitrate hexahydrate (218 mg, 0.75 mmol) and 1,3,5-benzenetricarboxylic acid (105 mg, 0.5 mmol) (btc) are gently warmed in 10 mL of resolved 1,2-propanediol (1,2-pd) [Avocado] until complete dissolution occurs. This stock solution is split into five equal portions and placed into 75 × 25-mm glass sample vials. Into each is placed a smaller sample vial, with a pierced lid, containing 5 drops of neat 3-picoline (3-pic) [or pyridine (py), **I**]. The larger vial is capped and sealed with laboratory film. The homochiral crystalline phases grow after approximately three weeks. Total yield = 450 mg (39% based on btc). Elemental analysis for **II**: $Ni_3(btc)_2(3\text{-pic})_6(1,2\text{-pd})_3$·$[(1,2\text{-pd})_9(H_2O)_{11}]$ $[Ni_3C_{90}H_{166}N_6O_{47}]$: Calculated C 47.82, H 7.40, N 3.72%; Found C 48.90, H 7.48, N 3.53% [based on a formula weight of 2260.37]. This formula is in excellent agreement with the desolvation data, and the estimated number of guests from the void electron population determined from the X-ray diffraction data by the method of Spek.[19]

Diffusion of pyridine or 3-picoline vapor into a solution of nickel (II) nitrate hexahydrate and 1,3,5-benzenetricarboxylic acid in 1-butanol with a concentration similar to those above, afforded crystals of **L** or **B**, respectively, within two weeks.

All attempts to grow phases from 3-functionalized pyridines with more electron-withdrawing substituents and 1,2-pd failed to give any solid product. In competition experiments with pyridine and 3-picoline in a 1:1 ratio present in 1,2-pd, only the 3-picoline phase, **II**, is obtained, as determined by the structural refinement of three single crystals.

Single-Crystal X-ray Diffraction Data. The single-crystal diffraction data were collected on five crystals of **II** grown from resolved R-diol and five crystals grown from resolved S-diol, on station 9.8 of the Synchrotron Radiation Source at Daresbury Laboratory and with a Bruker SMART CCD diffractometer. One synchrotron dataset was collected on a single crystal of **II** grown from racemic diol that had been desolvated under vacuum at room temperature as described below.

Representative crystal data for **II** at 150(2)K: $C_{63}H_{72}N_6Ni_3O_{18}$· (guests), $M = 1377.39$, blue blocks, 0.12 × 0.08 × 0.06 mm, cubic, space group $I4_132$, $a = 28.3174(4)$ Å, $V = 22707.0(6)$ Å^3, $Z = 8$, $\rho_{calcd} = 0.806$ g cm^{-3}, $\lambda = 0.6975$ Å, $\mu = 0.535$ mm^{-1}, minimum and maximum transmission 0.9386 and 0.9686, absorption corrected. 34032 reflections measured, 3245 unique, 3144 > $2\sigma(I)$ were used to refine 143 parameters, no restraints, to $R1$ ($wR2$) = 0.0435 (0.1212), Flack = 0.05(2), GOF = 1.173. Crystal data for desolvated **II′** at 150(2)K: $C_{63}H_{72}N_6Ni_3O_{18}$, $M = 1377.39$, blue blocks, 0.15 × 0.12 × 0.08 mm, cubic, space group $I4_132$, $a = 28.1350(4)$ Å, $V = 22\,271.1(5)$ Å^3, $Z = 8$, $\rho_{calcd} = 0.822$ g cm^{-3}, $\lambda = 0.6875$ Å, $\mu = 0.545$ mm^{-1}, minimum and maximum transmission 0.9227 and 0.9577, absorption corrected. 56 866 reflections measured, 3178 unique, 2934 > $2\sigma(I)$ were used to refine 139 parameters, no restraints, to $R1$ ($wR2$) = 0.0706 (0.2246), Flack = 0.02(3), GOF = 1.257. In both cases, structure solution was by direct methods (SHELXS-97)[20] and refined on F^2 in SHELXL-97.[21] All non-hydrogen atoms were refined anisotropically, and all hydrogen atoms were placed geometrically and refined with a riding model with U_{iso} constrained to be 1.2 (1.5 for methyl groups) times U_{eq} of the carrier atom. The hydrogen atoms of the 3-picoline methyl groups were allowed to freely rotate about the C−C bond. The diol moiety is split over two symmetry related sites as a consequence of the 2-fold symmetry about the metal center which occupies the *24 g* site, with the methyl group refined at half-occupancy. For both structures PLATON[19] was used to determine the extraframework volume by summing voxels more than 1.2 Å from the framework, and SQUEEZE[19] gave a void electron population of 478 for the solvated material (calculated 466 for 9 1,2-propanediol and 11 water molecules). The pore solvent in **II** is not crystallographically well-defined, and treatment of this residual electron density by the method of Spek modestly improves the fit of **II** (before SQUEEZE: $R1 = 0.0634$, $wR2 = 0.1956$ for 2948 data with ($I > 2sI$) and $R1 = 0.0687$, $wR2 = 0.2052$ for all data/restraint/parameters 3245/0/141). Crystallographic data (excluding structure factors) for **II** and **II′** have been deposited with the Cambridge Crystallographic Data Centre as supplementary publication numbers CCDC-225153 and CCDC-225154, respectively. Copies of the data can be obtained free of charge on application to CCDC, 12 Union Road, Cambridge CB2 1EZ, UK (Fax: (+44)1223-336-033; E-mail: deposit@ccdc.cam.ac.uk).

(18) Kepert, C. J.; Prior, T. J.; Rosseinsky, M. J. *J. Am. Chem. Soc.* **2000**, *122*(21), 5158−5168.

(19) Spek, A. L. *Acta Crystallogr., Sect. A* **1990**, *46*, C34.
(20) Sheldrick, G. M. *SHELXS-97*, Universitat-Gottingen, 1997.
(21) Sheldrick, G. M. *SHELXL-97*, Universitat-Gottingen, 1997.

Table 1. Unit Cell Parameters for Cells Regenerated by Resolvation of I′ with the Guest Species Given[a]

guest	refined cell/Å
as synthesized	28.848(7)
water	28.867(3)
methanol	28.84(1)
propan-1-ol	28.932(5)
propan-2-ol	28.929(5)
acetone	28.949(5)
butan-1-ol	28.861(9)
pentan-1-ol	28.967(4)
2-methylbutan-1-ol	28.979(2)
2-ethylbutan-1-ol	28.88(2)
1-phenylethanol *	29.013(3)
tetrahydrofuran	28.975(7)
toluene	28.918(4)
m-xylene	28.84(5)
cyclopentantol	28.80(2)
pyridine	layered **L** structure
3-picoline	28.747(1)

[a] Phenylethanol was employed over the bulk solid as a liquid.

Resolvation Chemistry. Samples of **I** rendered amorphous by heating to 150 °C under flowing nitrogen were ground and loaded into 0.5 mm Lindemann capillaries which were placed in sealed sample jars containing 0.5 mL of small volatile guest molecules (listed in Table 1). Samples were allowed to equilibrate with the vapor of these molecules at room temperature.

X-ray Powder Diffraction. Ambient temperature X-ray powder diffraction data were collected with Cu Kα_1 radiation with a Stoe Stadi-P diffractometer using a linear position sensitive detector. The evolution of the crystal structure of **I** upon desolvation was charted by an in situ energy-dispersive X-ray diffraction experiment performed on Station 16.4 of the SRS at Daresbury Laboratories. A sample was loaded onto a frit and heated to 150 °C at 2 °Cmin^{-1}, held at 150 °C for 5 min, cooled to 110 °C at 2 °Cmin^{-1} and then cooled to room temperature using a fan. Heating and cooling were carried out under a vertical flow of nitrogen at a flow rate of 80 cm^{3}min^{-1}. A single energy-dispersive X-ray diffraction spectrum was collected every 60s. A small portion of a NIST silicon standard powder was mixed with the sample. The intensity of the diffraction peaks due to this was monitored and these affirmed that the amount of sample in the sample chamber remained constant. A single detector set at $2\theta = 2.612$ ° was employed, allowing data collection in the range 15 to 2.5 Å.

Sorption Isotherm Measurement. All of the outgassing and isotherm measurements were carried out using a Hiden Isochema (Warrington U. K.) Intelligent Gravimetric Analyzer (IGA), equipped with a micro-gram balance, 2mbar, 100 mbar and 20 bar barotron pressure transducers and a Hüber ministat circulating water bath. For liquid nitrogen measurements, a standard low-temperature liquid dewar was employed. All isotherm data points were fitted by the IGASwin systems software v.1.03.84 (Hiden Isochema, 2002) using a linear driving force model when > 96% equilibration had been reached: all changes in sample weight were corrected for buoyancy effects. Samples of **II** were pipetted from the 1,2-pd mother liquor onto a sinter (diameter 30 mm, porosity 4), washed with a small portion of fresh 1,2-pd (resolved 1,2-pd if a homochiral material was under investigation) and dried at the pump for 60 min. The blue solids were scraped from the sinter using a micro-spatula, and ground in an agate mortar and pestle. The crystallinity of each sample was checked by X-ray powder diffraction, by examining the position and fwhm of the three most intense reflections, prior to any sorption measurement. Approximately 30−50 mg of sample was loaded onto the IGA and outgassed at 21 °C at pressures of 10^{-7} mbar until a constant mass had been reached; typically overnight. Mass losses were in the range 39−48% depending on how damp the samples were at loading. A similar method was employed for the preparation of **I**. If **II** is not ground prior to outgassing, then a single-crystal structure determination of the desolvated material, **II′**, can be obtained. Elemental analysis of **II′**: $Ni_3(btc)_2(3\text{-pic})_6(1,2\text{-pd})_3{\cdot}xH_2O$ [$Ni_3C_{63}H_{72+2x}N_6O_{18+x}$]: Calculated C 53.54, H 5.42, N 5.95% ($x = 2$); Found C 53.90, H 5.39, N 5.98% [the mass loss observed upon outgassing is consistent with the loss of all pore species, and the water molecules in this formula arise from the opening of the IGA air-admit valve when re-pressurizing the system prior to sample removal].

Scheme 1. Chiral Guest Species Used to Determine the Size-Dependent Enantioselectivity of II′; (i) Menthone, (ii) Fenchone, (iii) Ethyl-3-hydroxybutyrate, and (iv) Binaphthol.

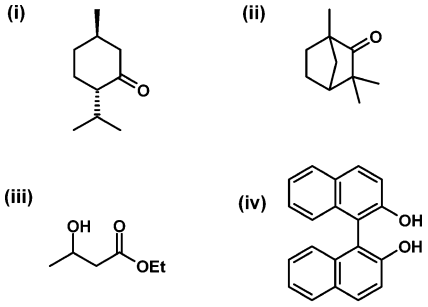

High-resolution nitrogen sorption data were collected in the pressure range 0.025−900 mbar at 77 K, with minimum and maximum logging times of 1 and 20 min, respectively, for each data point. Those data points that timed-out were each fitted manually off-line using the linear driving force model prior to any subsequent isotherm analysis.

For the vapor species ethyl-3-hydroxybutyrate (E3HB), 1,3,5-tri-isopropylbenzene (TIPB) [Lancaster synthesis] and perfluorotributyl-amine (PFBA) the vapor pressure constants were not readily available and were determined using the IGA equipment by measuring the saturated vapor pressure at three different temperatures and calculating from the Antoine equation. This was necessary in order to prevent condensation due to overpressure and to enable calculation of the relative pressure, p/p_0, at the sample. Each of the isotherms of the vapor species were measured at 306 K in the pressure ranges 0.01−1.05, 0.01 − 0.12 and 0.025−1.4 mbar for E3HB, TIPB and PFBA, respectively, with maximum logging times of 90 min and unfitted points treated as for the nitrogen data.

Uptake Experiments with Chiral Guest Species and Determination of Enantioselectivity. The chiral guest species chosen for the testing of enantioselectivity by the resolved framework **II′** were ethyl-3-hydroxybutyrate (E3HB), the terpenes menthone and fenchone and the aromatic diol binaphthol. (Scheme 1, i−iv) For E3HB, guest delivery was from the vapor phase, and for the terpenes from the liquid phase. Binaphthol was delivered from a dichloromethane (dcm) solution where the guest species was in a 5× molar excess.

All guests were delivered as racemic mixtures, either as obtained or by the preparation of an artificial racemate from the two resolved enantiomers. The enantiomeric excess (ee) of the racemic standards were determined before sorption by the framework and compared with the ee's obtained after removal from the framework. Extraction procedures for each guest are described in detail in the Supplementary Information. Ee's of E3HB and the terpenes were determined by chiral-GC using a Shimadzu GC-14B gas chromatograph equipped with a Lipodex-E column octakis(3-O-butanoil-2,6-di-O*n*-pentyl)-γ-cyclodex-trin stationary phase, and the ee's of binaphthol determined by chiral HPLC with a Waters 2695 Separations Module equipped with a Waters 996 Photodiode Array detector and a Chiralpak-AD column controlled and analyzed using the Millenium[32] analytical software package.

(22) Kepert, C. J.; Prior, T. J.; Rosseinsky, M. J. *J. Solid State Chem.* **2000**, *152*(1), 261−270.
(23) Steiner, T.; Desiraju, G. *Chem. Comm.* **1998**, 891−892.
(24) Dubinin, M. M.; Astakov, V. A.; Raduskevich, L. V. In *Physical Absorption of Gases and Vapors in Micropores*; Cadenhead, D., Danelli, J. F., Rosenberg, M. D., Eds.; Academic Press: New York, 1975; pp 1−70.
(25) McArdle, P. *J. Appl. Cryst* **1995,** 28, 65.

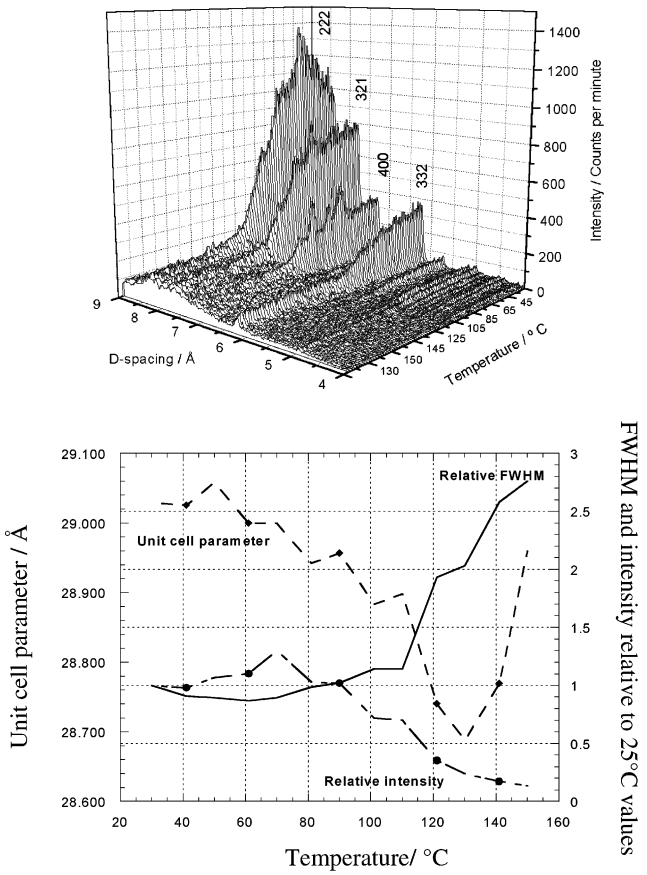

Figure 2. (i) The evolution of the X-ray powder diffraction pattern of **I** with temperature recorded in-situ with synchrotron radiation (Daresbury SRS, station 16.4). The Bragg peaks disappear at the temperature where thermal analysis indicates that the guests occupying the channels are lost. The diffraction pattern remaining after cooling to room temperature is that of **I′**.

Results

X-ray powder diffraction and gas sorption data show that the first-generation chiral open-framework solids **I** with pyridine and 1,2-propandiol as auxiliary ligands[18] collapse upon removal of the guests in the pore system and are thus not microporous. This is demonstrated in Figure 2, (i) where the evolution of the energy dispersive synchrotron powder X-ray diffraction pattern of $Ni_3(btc)_2(py)_6(1,2\text{-pd})_3\cdot[(1,2\text{-pd})_{11}(H_2O)_8]$ **I** with temperature reveals loss of crystallinity to afford amorphous **I′** above 130 °C, where thermal analysis demonstrates the loss of guests occupying the channels. With increasing temperature the 222 reflection first becomes sharper and more intense upon heating to approximately 80 °C (Figure 2(ii)). Above this temperature, it becomes much broader and diminishes in intensity.

(ii) Effect of desolvation on the 222 reflection of **I**. The solid line is the half width relative to that at 30 °C. The line with square markers is the unit cell parameter. The line with circular markers is the intensity of the 222 reflection relative to its intensity at 30 °C.

The unit cell parameter decreases in size with increasing temperature to 130 °C. After this point it appears to rise again, although at this temperature the 222 reflection has become broad and its center is poorly located. Similar structural collapse occurs upon removing the guests under vacuum at room temperature. (Figure S2) The crystallinity of the first generation porous chiral networks does not survive the loss of guests at room temperature.

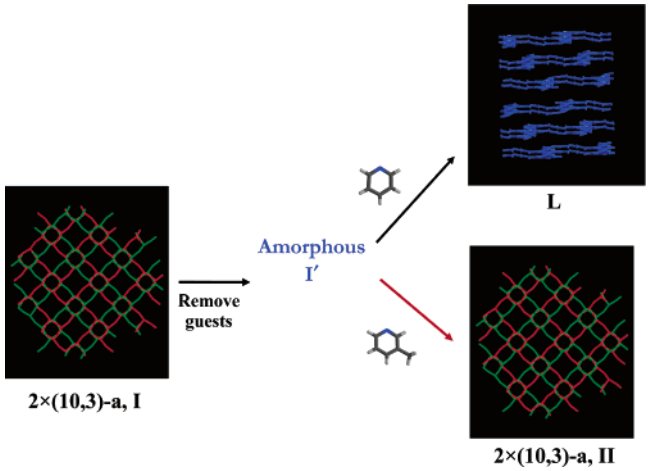

Figure 3. **I** contains two interpenetrating (10,3)-a nets of the same handedness, represented in green and red. The reaction of amorphous **I** (with small guest molecules affords crystalline materials—pyridine yields a nonporous layered structure L, whereas 3-picoline gives the 2((10,3)-a network structure initially adopted by **I**.

The resulting amorphous product **I′** is essentially nonporous to nitrogen and has a very low BET surface area. (12.63(8) $m^2 g^{-1}$). Despite the nonporous nature of **I′**, this amorphous solid is transformed into highly crystalline material upon reaction with small guest molecules, as described in Table 1. Most of the guests lead to reformation of the 2×(10,3)-a structure of **I**. The contrast between pyridine and 3-picoline in this resorption chemistry is particularly noteable (Figure 3). Reaction of **I′** with pyridine leads to a nonporous layered structure **L**,[22] in which the btc and Ni^{2+} centers form a two-dimensional (6,3) net. Reaction of **I′** with 3-picoline (3-methyl pyridine), however, affords solely the three-dimensional chiral 2×(10,3)-a structure.

The contrasting effectiveness of the pyridine and 3-picoline ligands in stabilizing the helical (10,3)-a network is further demonstrated by contrasting the structure formed by 1-butanol, Ni^{2+} and btc assembly in the presence of 3-picoline with that formed in the presence of pyridine. Growth from 1-butanol and pyridine affords $Ni_3btc_2(py)_6(^n\text{BuOH})_6\cdot[(^n\text{BuOH})_{2.2}(H_2O)_{6.5}]$ with the layered structure **L**. Growth from 1-butanol under identical conditions with 3-picoline in place of pyridine gives **B** $Ni_3btc_2(3\text{-pic})_6(^n\text{BuOH})_6\cdot$[guests] which adopts the chiral 2×-(10,3)-a network structure of **I**.

These observations suggested direct reaction of nickel nitrate with btc and 3-pic in 1,2-pd would generate a second generation of chiral networks with enhanced stability. Reaction affords **II** $Ni_3(btc)_2(3\text{-pic})_6(1,2\text{-pd})_3\cdot[(1,2\text{-pd})_9(H_2O)_{11}]$ with the 2×(10,3)-a network structure. The hand of the 1,2-propandiol used to prepare **II** strictly controls the helix chirality within the two interpenetrating (10,3)-a nets − studies on five crystals of both R- and S-templated material reveals right- (R-**II**) and left-handed (S-**II**) helices only, respectively, as defined by the refined Flack parameters (Table S1). The structural metrics of the unstable py **I** and stable 3-pic **II** phases are very similar, although the 2% decrease in unit cell volume upon adding the methyl group in **II** is surprising. It is noteable that the torsion of the 3-picoline methyl group about the C−C bond is well-defined and can be

(26) Cussen, E. J.; Claridge, J. B.; Kepert, C. J.; Rosseinsky, M. J. *J. Am. Chem. Soc.* **2002**, *124*, 9574−9581.

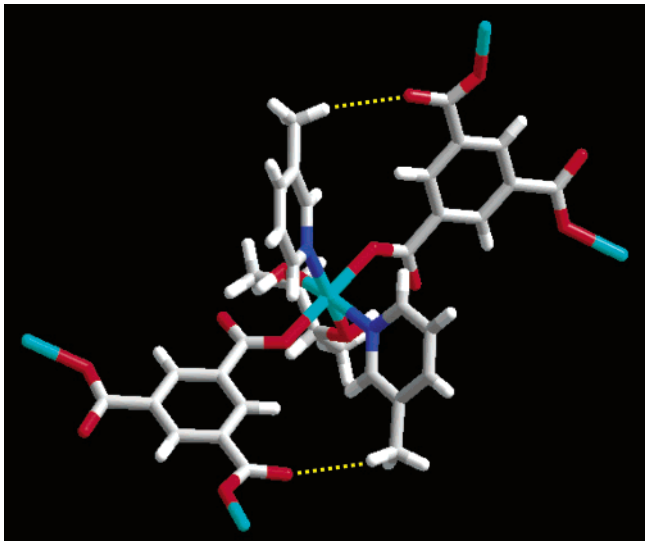

Figure 4. C−H···O interaction (yellow dotted line) between the methyl group of the 3-picoline auxiliary ligand and the nonbonding carboxylate oxygen atom (red) of the btc framework forming node in **II**. The Ni centers (light blue) and the btc ligands (trans to each other at the metal center) form the framework. The auxiliary ligands are two 3-picoline molecules (X) bound via the dark blue nitrogen atoms and one bidentate propan-1,2-diol (Y) at the rear of the picture.

refined against the synchrotron diffraction data, with the resulting orientation producing a C−H···O hydrogen bonding interaction with the oxygen atom of the carboxylate group that is not coordinated to the metal center[23] (d(H···O) = 2.768(2) Å, C−H···O = 153.5(3)°) (Figure 4). The 1-butanol phase **B** also displays these weak C−H···O interactions (d(H···O) = 2.55 Å, C−H···O= 167 °). ORTEP representations of the coordination around the metal center in **II** and **B** are given in Figure S3.

In strong contrast to **I**, heating **II** to 150 °C to drive off the guests results in a crystalline material **II′** with identical space group symmetry and slightly modified unit cell parameters (Figure S4, heating to higher temperatures results in loss of auxiliary ligands bound to the metal center and collapse of the structure). The Type I N_2 sorption isotherms (Figure 5(i)) for **II′**, desolvated at room temperature under high vacuum (Figure S5), revealed substantial nitrogen uptake and were identical after two sorption−desorption cycles, demonstrating the robustness of **II′**. Figure 5(i) also reports the N_2 sorption data for **I′**, demonstrating the nonporous nature of the first-generation material. The micropore-derived surface area of **II′** from high-resolution isotherm data (p/p_0 < 0.01) is 930(15) m^2/g. The Dubinin−Radushkevich[24] micropore volume of 0.63(1) ml g^{-1} corresponds well to the porosity estimate of 47% derived from the extraframework volume in the refined crystal structure and the estimated density of 0.8 g ml^{-1}. X-ray powder diffraction data from **II′** after the sorption isotherm measurements reveal no loss of crystallinity or transformation of structure upon guest loss and subsequent nitrogen sorption and desorption (Figure 5(ii)).

The stability of single crystals of **II′** allows refinement of the crystal structure of the desolvated homochiral porous material. Refinement of the Flack parameter shows that the **II′** structure retains homochirality, while refinement of the diol stereochemistry reveals the same relationship between the handedness of the helices and that of the diol template (in the

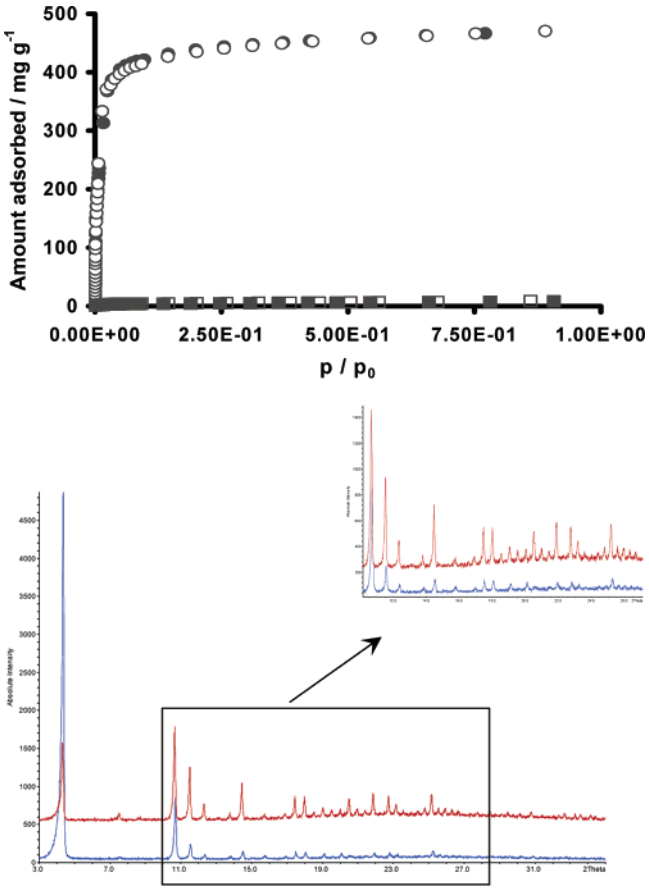

Figure 5. (i) 77K N_2 sorption (filled sphere) and desorption (empty spheres) isotherm of **II′** demonstrating the microporosity of the homochiral open framework. Square symbols represent N_2 sorption and desorption for nonmicroporous first generation **I′**. (ii) X-ray powder diffraction data for phase **II** (red upper) showing that upon guest removal under high vacuum conditions, the desolvated phase **II′** (blue lower) is highly crystalline. Refined cell parameters in $I4_132$: solvated (**II**) a = 28.693(11) Å, V = 23622.5(150) $Å^3$, desolvated (**II′**) a = 28.595(9), Å, V = 23382.1(128) $Å^3$. The inset shows that crystalline Bragg diffraction is maintained to short *d*-spacings.

crystal studied the R-diol gives a right-handed helix as expected with a refined Flack parameter of 0.01(3) in the absence of guests). The extracted electron density of zero in the extraframework volume indicates that all the guests have been removed from this crystal.[19] The C−H···O interaction identified as the single qualitative structural difference between **I** and the 3-picoline phase **II** is strengthened upon guest loss in **II′** as the methyl group rotates to make the C−H···O interaction closer to linearity (C−H···O = 164.9(5)°) and to shorten the contact distance to 2.665(3) Å.

Sorption isotherms were measured for the 1,3,5-trisisopropylbenzene (TIPB) and perfluorotributylamine (PFBA) probe molecules to allow comparison of effective pore diameters with well-characterized aluminosilicate open frameworks.[1] Both molecules are readily sorbed to similar levels by **II′** (0.44 mL g^{-1}, Figure 6), to give materials formulated as $[Ni_3(btc)_2(3\text{-pic})_6(1,2\text{-pd})_3]\cdot 2.5(TIPB)$ and $[Ni_3(btc)_2(3\text{-pic})_6(1,2\text{-pd})_3]\cdot 1.5(PFBA)$ based on total percentage uptake by mass. These large, relatively rigid guest molecules occupy 70% of the volume accessible to the much smaller N_2 probe. This ease of access of even the largest probe molecule used can be quantified by linear driving force model analysis of the uptake kinetics where

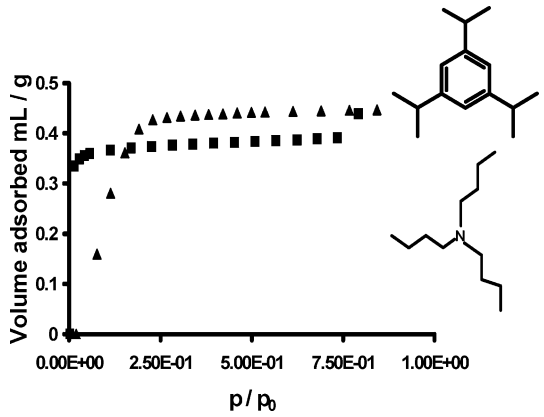

Figure 6. 300 K vapor sorption isotherms for guests 1,3,5-trisisopropylbenzene (triangular symbols) and perfluorotributylamine (square symbols) on **II′**. (in the schematic above, the fluorine atoms are omitted for clarity)

Table 2. Sorption Parameters for N_2 and Probe Molecule Studies Calculated by Fitting Isotherm Data for II′ to the Dubinin−Raduskevich Equation[a]

adsorbent	size/Å	W_o/mg g^{-1}	V_m/ml g^{-1}	βE_o/kJ mol^{-1}	T/ K
N_2	4	508.8(97)	0.630(12)	2.18(2)	77
TIPB	8.5	376.9(3)	0.446(1)	10.10(22)	306
PFBA	10.5	713.3(14)	0.379(1)	18.09(27)	306

[a] W_o is the total uptake, V_m is the micropore volume and βE_o is the interaction parameter.

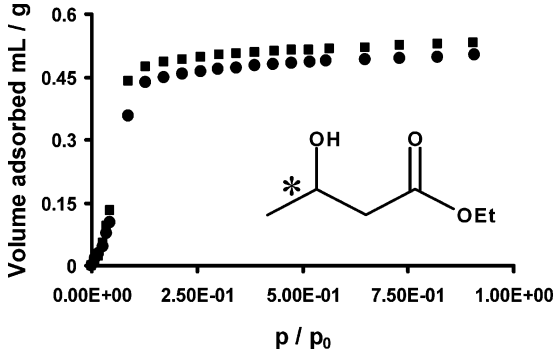

Figure 7. 300 K vapor sorption isotherms of R-ethyl-3-hydroxybutyrate by R-**II′** (circular symbols) and S-**II′** (square symbols), where the prefix indicates the hand of the 1,2-pd template used to prepare the host.

the time constants for >96% equilibration at $p/p_0 = 0.3$ only increase by a factor of 2 from N_2 (106(2) s) to the 1,3,5-trisisopropylbenzene (226(15) s) and perfluorotributylamine (266(30) s) probes. The sorption energies and pore volumes resulting from fitting all three probe molecule isotherms to the Dubinin−Raduskevich equation are shown in Table 2.

Figure 7 shows isotherms for uptake of R-ethyl-3-hydroxybutyrate by the two enantiomers of the host. Analysis with the Dubinin−Raduskevich equation reveals similar total uptake W_o (502(1) mg g^{-1} R-**II′**, 533(1) mg g^{-1} S-**II′**), micropore volume (0.494(1) ml g^{-1} R, 0.524(1) ml g^{-1} S) and adsorption energy (8.5(2) kJ mol^{-1} R, 9.1(2) kJ mol^{-1} S) for sorption of the R-ethyl 3-hydroxybutyrate guest. Sorbed ethyl-3-hydroxybutyrate vapor can be removed from the resolved frameworks **II** by washing with dichloromethane. X-ray powder diffraction reveals that removal of the guest species in this way does not alter the structure of the framework (Figure S6), further demonstrating the robust nature of this material. The "extracted" guest species can be identified by ^{1}H NMR or

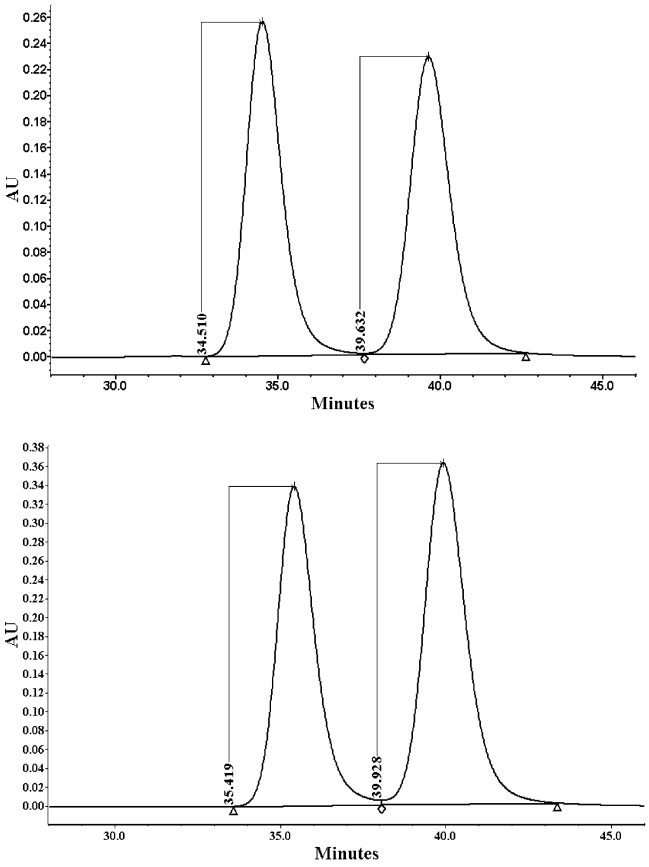

Figure 8. HPLC data of binaphthol: the upper diagram shows the peaks for the racemic (±)-binaphthol standard and the lower trace the binaphthol extracted from the pores of **S-II′**. The numbers marked are the elution times in minutes with R-binaphthol the first eluted species. R:S ratios and calculated enantiomeric excesses (ee's) are given in Table S4.

derivatized with trifluoroacetic anhydride (tfa) for chiral-GC analysis. Sorption of racemic ethyl-3-hydroxybutyrate vapor by the R- and S-frameworks, followed by removal and tfa derivatization in this way, shows no enantioselectivity within experimental error in either case. (Table S2)

This process of dichloromethane washing to remove guest molecules from the pores while maintaining framework integrity is easily applied to other chiral guest species and can also be exploited for the delivery of solid chiral guests into the desolvated phase **II′**. The terpene molecules menthone and fenchone are readily taken up by the framework from the liquid phase, and removed by dcm washing. While chiral-GC reveals no enantioselection for these larger chiral species (Table S3) the solid binaphthol guest is sorbed by microporous guest-free S-**II′** with an enantiomeric excess of 8.3% (as determined by HPLC analysis) in competition uptake experiments from a racemic mixture in dichloromethane solution (Figure 8, Table S4). The total amount of binaphthol sorbed by the desolvated material **II′** was determined as 7.3% uptake by mass (from the guests washed out from the binaphthol-loaded material) to yield a material with composition $[Ni_3(btc)_2(3\text{-pic})_6(1,2\text{-pd})_3]\cdot 0.35$-(binaphthol).

Discussion

The first-generation chiral open frameworks **I** contain helical networks that are insufficiently stable to retain their long-range order when the guests occupying the channels are removed.

Guest-free **I′** is poorly crystalline and does not sorb nitrogen, which demonstrates that the channels containing the guest in the as-grown material close when those guests are lost. The first-generation materials are thus not microporous. As these are structurally and compositionally complex materials, the identification of chemical modifications that will generate the enhanced stability required to generate microporous materials while retaining the chiral open-framework structure is not straightforward.

Suitable modifications to the components of **I** were identified by studying the reactivity of the amorphous **I′** phase formed on collapse of the first-generation systems toward small molecules. This reactivity following collapse after guest removal is characteristic of many metal-organic frameworks, and we have exploited it to identify a second generation of homochiral open-framework materials that are stable to guest loss and microporous in contrast to their first-generation parents **I**. The surprising contrast in the outcome of the reaction of **I′** with pyridine and 3-picoline allowed the identification of the compositional and structural features required to generate helical (10,3)-a nets that are stable to guest loss. Reaction of **I′** with pyridine in excess is expected to afford the layered phase **L** as this structure involves coordination of three pyridine molecules to the metal center,[22] rather than the two found in the chiral **I** frameworks. This transformation is driven by the strength of the pyridine coordination to the metal center. The observation that reaction of **I′** with 3-picoline, which differs only through the introduction of a methyl group in the 3-position, affords the chiral **I** structure was thus totally unexpected. It suggests that the chiral (10,3)-a network is strongly stabilized by the 3-picoline (3-pic) auxiliary ligand.

This was confirmed by the marked contrast in structure directing by the two nitrogen heterocycles in the presence of 1-butanol as the auxiliary ligand. Previous evidence strongly indicates that the **I** structure requires a bidentate diol bound to the metal for stability, and thus the competing layered structure **L** is expected to be formed with monodentate 1-butanol bound to the metal center when both pyridine and 3-picoline are the auxiliary ligands. The pyridine-containing phase does adopt this layered structure but binding of 3-picoline to the metal center drives the formation of the three-dimensional chiral two-network structure in **B**, the first time this has been observed without a bidentate diol. These observations demonstrate that the 3-picoline auxiliary ligand stabilizes the (10,3)-a network.

The selection of the chiral (10,3)-a structure by the 3-picoline auxiliary ligand suggested that the thermal stability and robustness to guest loss of the first-generation homochiral phase **I** would be enhanced by replacing pyridine with 3-picoline as auxiliary ligand X in the second generation **II** phases. This is confirmed by the demonstration of microporosity in the desolvated **II′** phase by gas sorption and the robustness of the crystal structure to guest loss. The sorption and diffraction measurements in Figure 5 show that a homochiral microporous material has been prepared.

The enhanced stability of the guest-free microporous homochiral material **II′** must originate in the replacement of pyridine with 3-picoline in the coordination sphere of M. The increased basicity of the alkyl pyridine is not responsible, as phases with 4-picoline as auxiliary ligand collapse upon guest removal. The C−H···O interaction between the methyl group of the 3-picoline and the nonbonding oxygen of the btc carboxylate group is the only clear structural difference between the unstable first-generation **I** and stable second-generation **II** phases, and it is responsible for the enhanced stability of the 3-picoline-based chiral phases. The stability of single crystals of **II** to guest loss permits the refinement of the homochiral microporous structure **II′** in the absence of guests.

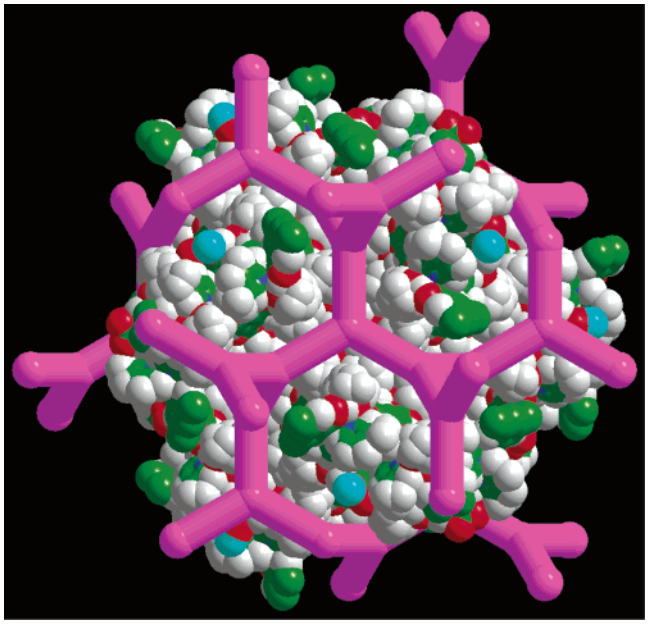

Figure 9. Three-dimensional chiral channel and pore system in **II′** is represented by voids centered on the 8b positions in $I4_132$ (purple spheres) connected by bonds to represent the channel system which forms a (10,3)-a network.

The C−H···O interaction is increased in directionality and decreased in length upon guest loss from **II** to afford **II′**, with rotation of the methyl group to enhance the strength of the interaction resulting in the stabilization of the helical network structure and the establishment of permanent chiral porosity. This interaction is sufficient to stabilize the network against collapse when the guests in the pores are removed and drives the observed contraction in cell volume from **I** to **II** upon the addition of the methyl group.

The chiral channels and pores in **II** are zigzag rather than straight in nature and thus difficult to visualize directly. Using the ORTEX software package,[25] the extraframework volume in the material was determined by placing void atoms at points further than 1.2 times the van der Waals radius from a given atom. The porosity of **II′** is a three-dimensional channel system passing through the centers of the 8b special positions in the $I4_132$ space group. The porosity thus describes a chiral (10,3)-a network itself defined by the doubly interpenetrating (10,3)-a nets that constitute the framework of the material (Figure 9). The helical nature of the extraframework porosity [25] is shown in Figure 10, where it is superimposed upon the (10,3)-a network connecting the pore centers.

Vapor sorption of guest molecules of defined diameters allows determination of the pore dimensions of the open chiral framework. The 1,3,5-trisisopropylbenzene and perfluorotributylamine probe molecules have dimensions of 8.5 Å and 10.5 Å respectively. The extent of uptake both demonstrates the large pores present in the material directly (the channels have dimensions > 1 nm) and shows that 30% of the porosity is

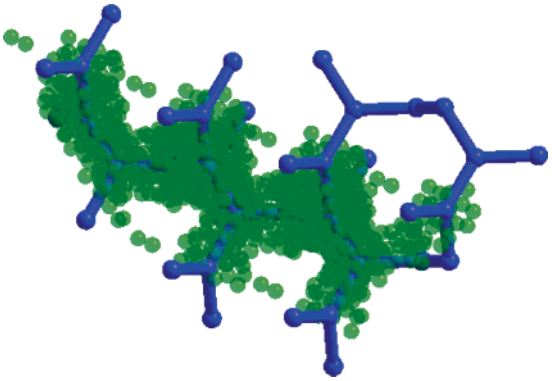

Figure 10. Extraframework porosity of **II′** is represented by the green transparent spheres at points further than 1.2 times the van der Waals radius from a given framework atom. The 8b positions which mark the center of the voids are represented by blue spheres connected by blue rods to illustrate the channel system. The vectors connecting the pore centers lie along the ⟨110⟩ directions.

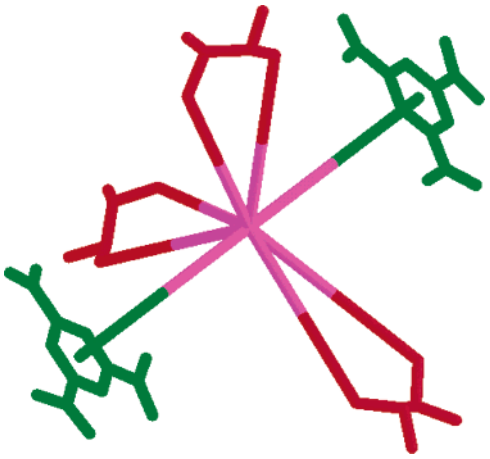

Figure 11. Closest contacts between the 8b pore centers of the extraframework volume of **II′** and the two interpenetrating networks of framework atoms. The atoms in the two networks are represented in green and red to distinguish the two components of the framework. The 8b pore centers (purple) are defined by close contacts to atoms from both of the interpenetrating (10,3)-a nets that make up the structure of **II**. The closest interatomic contacts to an atom at the pore center would be 6.32 Å to the hydrogen atoms of the 1,2-pd methyl groups (from network one, shown in red). The more distant contacts to the carbon atoms of the btc nodes of the second network (shown in green) define the pore.

accessible only to molecules smaller than 1,3,5-trisisopropylbenzene. The closest contacts to the framework from the pore centers (Figure 11) are to the methyl groups of three 1,2-pd molecules from one of the two (10,3)-a networks, forming an inherently chiral lining to the channels. The close contacts to the hydrogen atoms of the 1,2-pd molecules suggest a 10.6 Å kinetic diameter for the pores; narrowing of this contact distance to 5.26 Å along the interpore vectors lying along ⟨110⟩ gives an 8.5 Å estimate for the narrowest point of the channels. Channel and pore estimates are given between the van der Waals surfaces of the atoms, not as center-to-center distances. However it should be noted that the distance to the carbon atom of the 1,2-pd methyl group is 6.13 Å and to the carbon bearing the group itself is 6.78 Å − given the conformational flexibility expected in the five-membered ring formed by the 1,2-pd bound to the Ni center and the rotation possible around the C−C bond to minimize limiting contacts to the methyl hydrogens (this group, unlike the methyl group of the 3-picoline is not locked into position by structurally important nonbonded contacts to other parts of the framework), kinetic diameters of 12 Å or higher can be expected for the channels given the flexibility displayed by metal-organic frameworks in sorbing guests.[26] More rigid contacts can be identified between the 8b pore centers and the btc framework nodes from the second helical (10,3)-a network; unlike the contacts to the conformationally flexible five-rings formed by the 1,2-pd auxiliary ligands, the 8.24 Å distances to the benzene carbon atoms of the network-forming btc ligands are less likely to relax in the presence of a guest. This gives an estimate for the pore diameter of 13.6 Å. The three-dimensionality of the chiral pore system is consistent with the kinetically facile sorption of large guest molecules, and the ready sorption of the 10.5 Å probe molecule is consistent with the larger estimates of the pore diameters that take into account the inherent flexibility of the components of the molecular network.

The large chiral pores and channels give a selectivity for chiral guest molecules that depends strongly on their size. Small volatile molecule uptake is readily investigated by vapor sorption, and the uptake of ethyl 3-hydroxybutyrate (smallest dimensions 6 × 3 Å) is only slightly sensitive to the host handedness for a defined enantiomer (R) of the guest. Menthone (8 × 5 Å) and fenchone (5 × 4 Å) are still too small compared to the channel dimensions to display appreciable enantioselection. The largest chiral guest tested is binaphthol which, although its perpendicular dimensions at 9 × 9 Å are smaller than both the estimated and minimum measured channel diameter, is sorbed by microporous guest-free S-**II′** with an enantiomeric excess of 8.3% in competition uptake experiments from a racemic mixture in dichloromethane solution. The stable homochiral microporous material is thus capable of enantioselective sorption to an extent dependent on guest size. A close match to the channel dimensions is required to bring the chiral guests sufficiently close to the helical internal surface of **II′** to allow for discrimination between the enantiomers. Establishing the size-shape-functionality requirements for enhanced enantioselection by **II′** will require considerable and detailed further work.

Conclusion

The stabilization of chiral framework topologies such as the (10,3)-a network rather than the use of chiral building blocks is an alternative strategy in the search for chiral open-framework materials. The generation of homochiral crystalline microporous materials from such structures requires the isolation of specific structural features. The loss of the guests from the second-generation phase **II** allows the multiple C−H···O interactions, which favor the formation of the helical framework when 3-picoline is the auxiliary ligand X, to become stronger in the desolvated material **II′**, thus stabilizing the chiral porosity. The identification of the weak but necessary interactions between the framework-forming components of the material and the auxiliary ligands bound to the metals was made using reactive selection from an amorphous intermediate which formed upon collapse of the structure when the guests are removed. Amorphous and nonporous phases such as **I′** are often formed by guest loss from unstable metal-organic frameworks. As the examination of the outcome of the reaction of the amorphous intermediate with small molecules resulted in the identification of a surprising contribution to stabilizing the chiral open

framework structure, this reactive selection of stable frameworks could become a useful route to identifying robust examples of metal-organic open-framework materials. The identification of a permanently microporous crystalline chiral open framework with nanometer-sized helical channels from readily available starting materials demonstrates that metal-organic frameworks can give access to qualitatively new functionality in microporous materials.

Acknowledgment. The authors acknowledge M. Pursglove for assistance with HPLC analysis and S. Teat (SRS Daresbury) and J. Bickley (University of Liverpool) for X-ray data collection. EPSRC supported this work under GR/N08537. The IGA instrument forms part of the North West Molecular Materials Centre supported by the EPSRC.

Supporting Information Available: ⟨111⟩ view of the (10, 3)-a network. Sample preparation for enantiomeric excess determination. X-ray powder diffraction from solvated and desolvated **I**. Refined Flack parameters for R- and S-templated crystals of **II**. ORTEP representations of the structures of **II** and **B**. X-ray powder diffraction pattern of thermally desolvated **II**. Evolution of the mass of **II** upon outgassing under high vacuum. GC data for menthone and isomenthone sorption. X-ray powder diffraction data showing the stability of **II** throughout the procedure of guest (ethyl 3-hydroxybutyrate) uptake and removal. Dubinin−Raduskevich plots for sorption of guest vapours by **II′**. This material is available free of charge via the Internet at http://pubs.acs.org.

JA0316420